Construction of an Electrostatic Beamline for Low-Energy Antiprotons to Carry Out Laser Spectroscopy of Antiprotonic Helium

Karin Watanabe
Supervisor: Dr. habil. Masaki Hori

23th August 2023

Abstract

CERN's ASACUSA experiment produces antiprotonic helium atoms [1] and precisely measures the atomic transition frequencies by laser spectroscopy. By comparing the measured frequencies with the results of quantum electrodynamics calculations, the antiproton-to-electron mass ratio can be determined. I primarily constructed the electrostatic beamline to transport ultra-slow antiprotons from the ELENA storage ring to the experimental helium target where the exotic atoms were formed.

1 Introduction

In 2021, CERN began operation of a new synchrotron facility called ELENA to decelerate antiprotons. Here a pulsed beam containing some 10^7 antiprotons is produced every 120 seconds by bombarding an iridium target with a proton beam. The antiprotons are then gradually decelerated to a kinetic energy of 100 keV. Electron cooling is applied by elastically scattering the antiprotons off of a co-moving electron beam, so that the velocity spread of the antiprotons circulating in ELENA is reduced to 0.1% or less.

In the ASACUSA experiment [2, 3, 4, 5], the 100 keV antiproton beam was injected into a helium gas target which was maintained at a temperature of 1.6 K and a pressure of less than 100 Pa. An antiprotonic helium atom was formed when one of the electrons orbiting a helium nucleus was replaced by an antiproton. The antiproton occupied a highly-excited Rydberg state with a principal quantum number $n \approx 38$ and an orbital angular momentum quantum number $\ell \approx 37$. When the antiprotonic helium atom was irradiated with laser light having an optical frequency corresponding to the atom's transition energy, a laser resonance occurred and the orbital antiproton deexcited to a lower energy state. Our aim is to determine the antiproton-to-electron mass ratio with a precision of about 12 digits by comparing the transition frequencies of this atom to the results of quantum electrodynamics calculations.

When the vacuum inside the ELENA synchrotron deteriorated to levels much above 10^{-12} mb, the antiprotons that circulate in ELENA collided with the atomic nuclei comprising the residual gasses so frequently that the antiprotons annihilated before the electron beam cooling could be completed. On the other hand, only an ultra-thin 1 µm thick Mylar window separated the helium gas in the experimental target and the antiproton beam line to allow the passage of the 100 keV antiproton beam. Last year a new beamline was constructed, but during tests helium gas permeated through the Mylar window and contaminated the synchrotron. As ELENA incorporated ion pumps with particularly low pumping speeds against helium, the vacuum inside ELENA deteriorated and 25% of the circulating antiprotons were lost. For this reason, my supervisor and I constructed a 8-meter long, ultra-high vacuum beamline (see Fig. 1) with differential pumping which transported antiprotons to the target without allowing the backflow of excessive helium gas into ELENA.

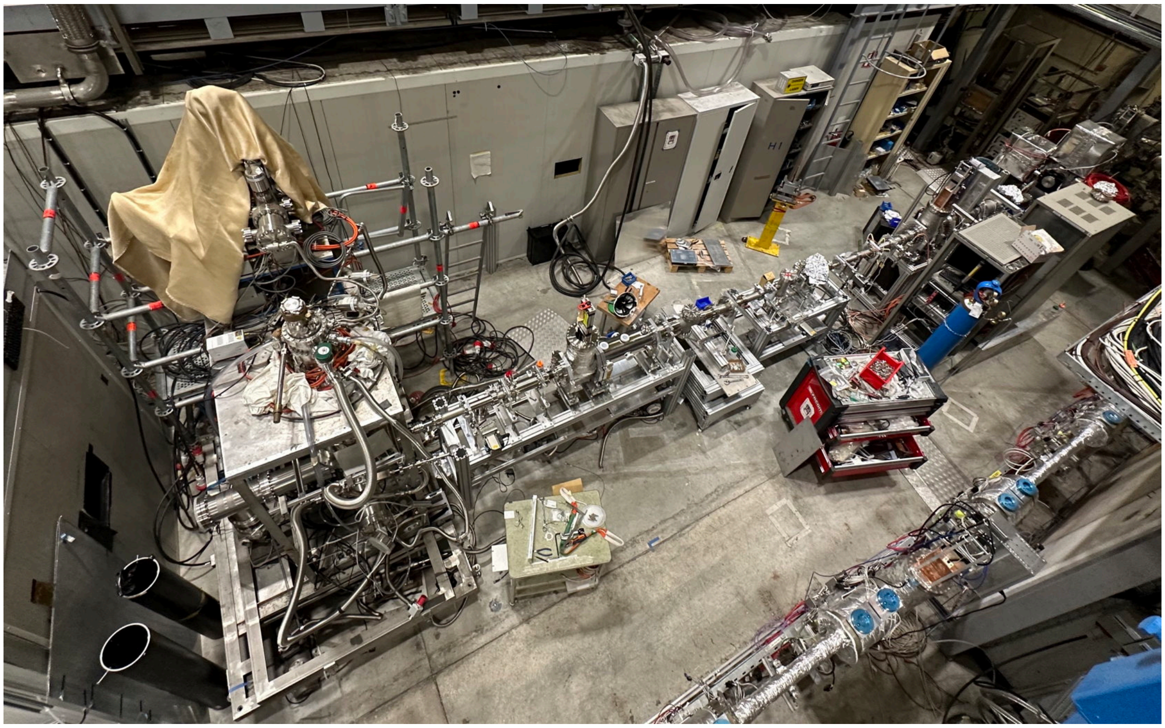

Figure 1: Wide-angle photograph of electrostatic beamline constructed by us.

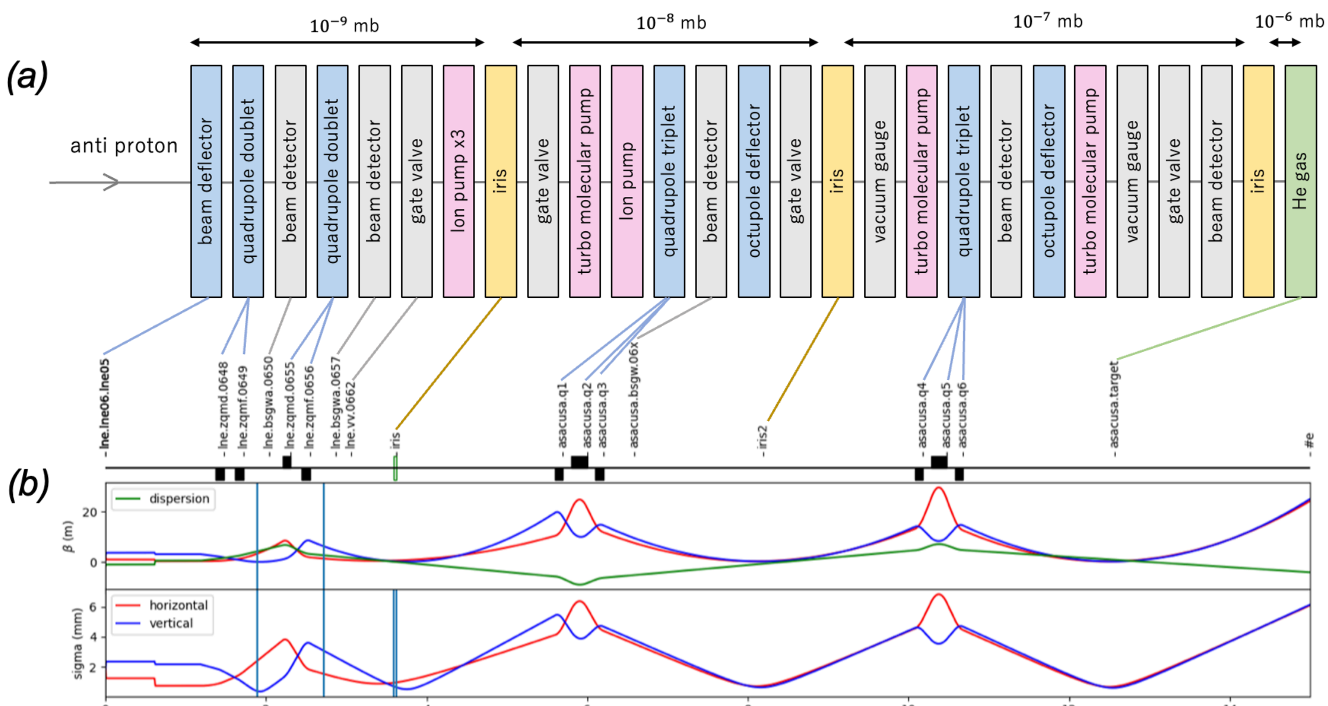

Figure 2: (a): Schematic block diagram of the beamline showing the sequence of various parts, (b) Optical trajectory of the new beamline constructed by us and simulated by the TE-ABT-BTP group. The horizontal and vertical β-functions and root-mean-square (RMS) beam size radii are shown.

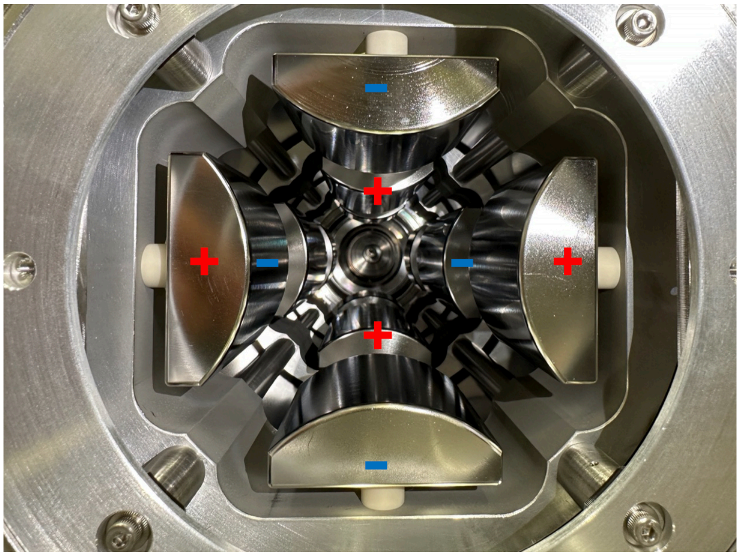

Figure 3: Photograph showing the internal structure of the quadrupole triplet. Electrodes with positive and negative voltages applied on them are indicated.

Figure 4: Photograph of the electrode structure of the octupole deflector.

2 Electrostatic beamline

2.1 Design overview

Fig. 2(a) shows the schematic block diagram of the beamline. Three irises placed at intervals of 4 m along the beamline subdivided the vacuum chambers that comprised the beamline into four sections. Five turbomolecular pumps with pumping speeds of between 80 L/s and 300 L/s, and six ion pumps capable of pumping noble gasses were installed between the irises to establish the differential pumping. Each iris constituted a stainless steel tube with an inner diameter of 9 mm and a length of 76 mm. The irises were ultrasonically cleaned and sealed on polished copper flanges using indium wires. The irises strongly limited the flow of gas from the experimental target to ELENA, since the conductance of gas undergoing molecular flow is proportional to the cube of the tube diameter and inversely proportional to its length. The total beamline length of 8 m also contributed to reducing the conductance. A vacuum gate valve installed just upstream of the helium target was briefly opened in sychronization with the arrival of the antiprotons at the helium target to further reduce the effective amount of escaping helium gas. We thus expected to reach vacuum levels of 10^{-9} mb, 10^{-8} mb, 10^{-7} mb, 10^{-6}mb in the four consecutive sections of beamline from the synchrotron to the target.

The beamline contained conflat vacuum flanges with various diameters between 34 and 260 mm. The flanges and inner chamber walls were carefully cleaned with acetone and methanol using a lint-free sponge. The vacuum was measured by cold cathode gauges with triaxial readout cables. I assembled three aluminium support frames with lengths of between 1 and 2 m. I then installed some support mounts that incorporated fine-motion mechanisms on the frames, and carefully placed the vacuum chambers on the mounts. It was particularly difficult to install, align, and close the quadrupole triplets and ion pumps that weighed between 20 and 40 kg. It required the cooperation of CERN's crane operation teams.

2.2 Quadrupole triplets

According to the measurements carried out last year, the emittance of the antiproton beam ejected from ELENA was about $\epsilon = 5\ \pi$ mm mrad. The beamline contained two pairs of quadrupole doublets, two quadrupole triplets, and two octopole deflectors to transport the beam to the target and prevent the antiprotons from colliding with the inner walls of the irises. The antiproton beam that propagated along the axis of the quadrupole triplet underwent alternating convergence and divergence in the horizontal and vertical beam planes; this resulted in a net focusing effect due to the so-called "principle of strong focusing".

Fig. 3 shows a photo of the inner structure of the quadrupole triplet. In each quadrupole, four hyperboloid-shaped electrodes were placed parallel and equidistantly from the beam axis at distances of 25 mm. Three sets of such quadrupoles were arranged along the beam axis. Voltages of ±6 kV were applied to the 12 electrodes to generate the quadrupole triplet field. A doublet, on the other hand, contained two sets of quadrupole electrodes which allowed less flexibility in correcting for the net aberrations introduced by the electrostatic beamline.

2.3 Octupole deflector

The two sets of octupole deflectors each consisted of a split cylindrical electrode with an inner diameter of 50 mm made of stainless steel (see Fig. 4). Each cylinder was subdivided into eight equal segments along the axial direction. The trajectory of the antiproton beam was adjusted by applying voltages of ±200 V to the electrodes to generate an uniform and perpendicular electric field near the axis of the cylinders. Compared to a simple deflector that contains only two sets of parallel plates, the aberrations of the electric field were improved by about two orders of magnitude. In order to generate the eight channels of high voltage, inverting amplifiers with a gain of 20 that incorporate high-voltage operational amplifiers were used.

2.4 Wire beam profile detector

Three secondary electron emission detectors based on wire grids with diameters between 10 and 20 μm were installed so that the diameter of the antiproton beam could be measured at three locations along the beamline.

3 Beam trajectory simulation results

Fig.2(b) shows the results of a trajectory simulation of the antiproton beam propagating along the beamline. The horizontal axis indicates the axial coordinate s along the beamline in meters. The 100 keV antiprotons are transported from the left side to right in the figure. The standard deviation of the cross section of the beam which is assumed to have a Gaussian profile is denoted by σ, whereas the so-called beta function $\beta(s)$ is related to σ by the relation, $\sigma(s) = \sqrt{\epsilon \cdot \beta(s)}$. By carefully adjusting the focusing voltages of the quadrupole doublets and triplets, the beam size near the irises and target were reduced to $\sigma \approx 1$ mm.

4 Future perspectives

In this year's beamtime, we will demonstrate the performance of our beamline and carry out high-precision laser spectroscopy of antiproton helium. In collaboration with the accelerator division of KEK, we will furthermore develop a device that incorporates nanocrystalline soft magnetic materials of iron-based amorphous alloys to decelerate antiprotons, and place it in the beamline.

References

[1] V. I. Korobov, L. Hilico, J.-P. Karr, $m\alpha^7$-order corrections in the hydrogen molecular ions and antiprotonic helium, *Phys. Rev. Lett.* **112**, 103003 (2014).

[2] M. Hori et al., Two-photon laser spectroscopy of antiprotonic helium and the antiproton-to-electron mass ratio, *Nature* 475, 484 (2011).

[3] M. Hori et al., Buffer-gas cooling of antiprotonic helium to 1.5 to 1.7 K, and antiproton-to − electron mass ratio, *Science* 354, 610 (2016).

[4] M. Hori, H. Aghai-Khozani, A. Sótér, A. Dax, D. Barna, Laser spectroscopy of pionic helium atoms, *Nature* 581, 37 (2020).

[5] A. Sótér, H. Aghai-Khozani, D. Barna, A. Dax, L. Venturelli, M. Hori, High-resolution laser resonances of antiprotonic helium in superfluid ^{4}He, *Nature* 603, 411 (2022).